

# Experiments and Modeling of the Autoignition of Methyl Pentanoate at Low to Intermediate Temperatures and Elevated Pressures in a Rapid Compression Machine

Bryan W. Weber<sup>a,\*</sup>, Justin A. Bunnell<sup>a</sup>, Kamal Kumar<sup>b</sup>, Chih-Jen Sung<sup>a</sup>

<sup>a</sup>*Department of Mechanical Engineering, University of Connecticut, Storrs, CT, USA*

<sup>b</sup>*Department of Mechanical Engineering, University of Idaho, Moscow, ID, USA*

---

## Abstract

Methyl valerate ( $\text{C}_6\text{H}_{12}\text{O}_2$ , methyl pentanoate) is a methyl ester and a relevant surrogate component for biodiesel. In this work, we present ignition delays of methyl valerate measured using a rapid compression machine at a range of engine-relevant temperature, pressure, and equivalence ratio conditions. The conditions we have studied include equivalence ratios ( $\phi$ ) from 0.25 to 2.0, temperatures between 680 K and 1050 K, and pressures of 15 bar and 30 bar. The ignition delay data demonstrate a negative temperature coefficient region in the temperature range of 720 K–800 K for both  $\phi = 2.0$ , 15 bar and  $\phi = 1.0$ , 30 bar, with two-stage ignition apparent over the narrower temperature ranges of 720 K–760 K for 15 bar and 740 K–760 K at 30 bar. In addition, the experimental ignition delay data are compared with simulations using an existing chemical kinetic model from the literature. The simulations with the literature model under-predict the data by factors between 2 and 10 over the entire range of the experimental data. In addition, a new chemical kinetic model is developed using the Reaction Mechanism Generator (RMG) software. The agreement between the experimental data and the RMG model is also not satisfactory. To help determine the possible reasons for the disagreement, a path analysis of both models is completed. It is found that improvements to both the reaction

---

\*Corresponding Author: bryan.weber@uconn.edu

pathways and thermodynamic properties are required. Further directions for future improvement of the methyl valerate model are discussed.

*Keywords:* chemical kinetics, rapid compression machine, autoignition, methyl ester, methyl valerate, methyl pentanoate

---

## 1. Introduction

For transportation applications, biodiesel is an important constituent in improving environmental friendliness of fuels. This is due to its renewability when produced from sustainable agricultural crops and its ability to reduce emissions relative to petroleum-derived fuels [1]. Biodiesel typically consists of long-chain methyl ester molecules, with typical compositions of  $C_{14}$  to  $C_{20}$  [1]. Recognizing that the large molecular size of the methyl esters within biodiesel fuel makes creating and using detailed chemical kinetic models challenging [2], it is desired to study their combustion chemistry by studying simpler methyl ester molecules.

A recent review paper summarizes the work on methyl esters relevant to biodiesel combustion [3]; the following summary focuses on ignition delay measurements, since these are the focus of this paper. Autoignition of methyl butanoate (MB,  $C_5H_{10}O_2$ ) has been well-studied in both shock tube and rapid compression machine experiments [4–10]. The prevalence of MB data in the literature is largely due to the early identification of MB as a potential surrogate fuel for biodiesel [11]. However, the literature experiments have shown that MB may not be an appropriate surrogate for biodiesel, due to its lack of negative temperature coefficient (NTC) behavior, a requirement for a suitable biodiesel surrogate [3].

Methyl esters larger than MB, such as methyl valerate (MV,  $C_6H_{12}O_2$ , methyl pentanoate), have also been studied as possible biodiesel surrogates. Hadj-Ali et al. [9] used a rapid compression machine (RCM) to study the autoignition of several methyl esters including MV. Although MV exhibited two-stage ignition in this study, little additional research has been done on its low-

26 temperature chemistry. Korobeinichev et al. [12] studied MV in premixed lam-  
 27 inar flames and extended a detailed high temperature chemical kinetic model  
 28 to include MV and methyl hexanoate. Dmitriev et al. [13] added MV to n-  
 29 heptane/toluene fuel blends to determine the resulting intermediate species in  
 30 premixed flames using a flat burner at 1 atm and an equivalence ratio of 1.75.  
 31 The addition of MV helped reduce soot forming intermediates including ben-  
 32 zene, cyclopentadienyl, acetylene, propargyl, and vinylacetylene [13]. Hayes  
 33 and Burgess [14] computationally examined the peroxy radical isomerization  
 34 reactions for MV to better understand the low temperature reaction pathways.  
 35 Finally, Diévar et al. [15] used diffusion flames in the counterflow configuration  
 36 to determine extinction limits for a number of methyl esters, including MV, and  
 37 validated a detailed kinetic model with the experimental data.

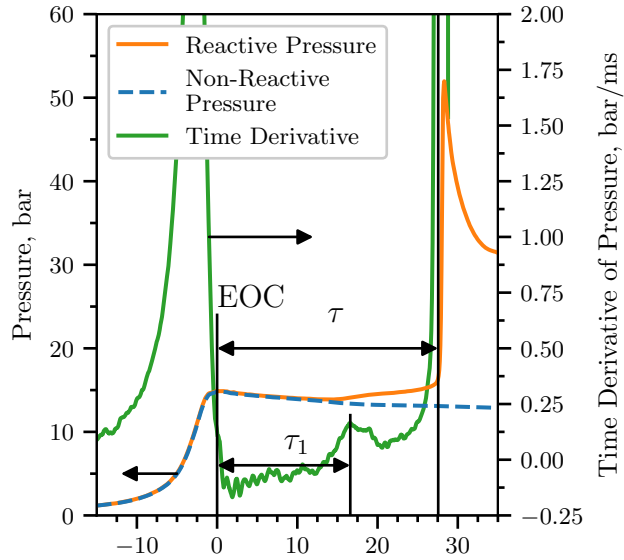
38 This work provides additional data for the autoignition of MV. Data is col-  
 39 lected in a RCM under engine relevant conditions spanning from 15 bar to 30 bar,  
 40 equivalence ratios ( $\phi$ ) from 0.25 to 2.0, and temperatures from 680 K to 1050 K.  
 41 The NTC region of MV is mapped out to provide additional information on the  
 42 fidelity of using MV as a biodiesel surrogate and insights into the autoignition  
 43 chemistry of large methyl esters.

## 44 **2. Experimental Methods**

45 The RCM used in this study is a single piston arrangement and is pneu-  
 46 matically driven and hydraulically stopped. The device has been described in  
 47 detail previously [16] and will be described here briefly for reference. The end  
 48 of compression (EOC) temperature and pressure ( $T_C$  and  $P_C$  respectively), are  
 49 independently changed by varying the overall compression ratio, initial pressure  
 50 ( $P_0$ ), initial temperature ( $T_0$ ), and specific heat ratio of the experiments. The  
 51 piston in the reaction chamber is machined with a specially designed crevice to  
 52 suppress the roll-up vortex effect and promote homogeneous conditions in the  
 53 reactor during and after compression [17].

54 The primary diagnostic on the RCM is the in-cylinder pressure measured by

55 a Kistler 6125C dynamic transducer that is compensated for thermal shock. The  
 56 transducer is coupled to a Kistler 5010B charge amplifier. The voltage output  
 57 of the charge amplifier is recorded by a National Instruments 9125 analog input  
 58 device connected to a cDAQ 9178 chassis. The voltage is sampled at a rate of  
 59 either 50 kHz or 100 kHz by a LabView VI and processed by a Python package  
 60 called UConnRCMPy [18]. Version 3.0.5 of UConnRCMPy [19], 3.6 of Python,  
 61 2.3.0 of Cantera [20], 1.13.0 of NumPy [21], 0.19.0 of SciPy [22], and 2.0.1 of  
 62 Matplotlib [23] are used in the analysis in this paper.



63

Figure 1: Definition of the ignition delays used in this work. The experiment in this figure  
 is conducted for a  $\phi = 2.0$  mixture with  $\text{Ar}/(\text{N}_2 + \text{Ar}) = 0.5$ ,  $P_0 = 0.7806$  bar,  $T_0 = 373$  K,  
 $P_C = 14.92$  bar,  $T_C = 720$  K,  $\tau = (27.56 \pm 0.89)$  ms, and  $\tau_1 = (16.60 \pm 0.46)$  ms. The non-  
 64 reacting pressure trace by replacing  $\text{O}_2$  with  $\text{N}_2$  is also shown for reference.

65 The compression stroke of the RCM brings the fuel/oxidizer mixture to the  
 66 EOC conditions, and for suitable thermodynamic states, the mixture will ignite  
 67 after a delay period. The definitions of the ignition delays are shown in Fig. 1.  
 68 The time of the EOC is defined as the maximum of the pressure trace prior to  
 69 the start of ignition and the ignition delays are defined as the time from the EOC

until local maxima in the first time derivative of the pressure. Each experimental condition is repeated at least five times to ensure repeatability of the data. As there is some random scatter present in the data, the standard deviation ( $\sigma$ ) of the ignition delays from the runs at a given condition is computed. Typically,  $\sigma$  is less than 10 % of the mean values of the overall ignition delay ( $\tau$ ) and the first stage ignition delay ( $\tau_1$ ).

In addition to the reactive experiments, non-reactive experiments are conducted by replacing  $O_2$  with  $N_2$  to determine the influence of machine-specific behavior on the experimental conditions (see Fig. 1) and permit the calculation of the EOC temperature via the isentropic relations between pressure and temperature [24]. The EOC temperature is calculated by the procedure described in Section 3.

The mixtures considered in this study are shown in Table 1. Four equivalence ratios of MV in “air” are considered. While  $O_2$  is kept at 21 % by mole in the oxidizer, the ratio of Ar :  $N_2$  in the oxidizer is varied to adjust the temperatures reached at the EOC. Two  $P_C$  conditions are studied in this work, 15 bar and 30 bar, representing engine-relevant conditions. For the  $\phi = 2.0$  condition, only  $P_C = 15$  bar is considered because we could not achieve  $T_C$  values low enough that the ignition during the compression stroke can be prevented.

Table 1: Mixtures considered in this work

$\phi$	Mole Fraction (purity)				Ar/( $N_2 + Ar$ )
	MV (100 %)	$O_2$ (99.994 %)	Ar (99.999 %)	$N_2$ (99.999 %)	
0.25	0.0065	0.2087	0.7848	0.0000	1.0
0.5	0.0130	0.2074	0.7796	0.0000	1.0
1.0	0.0256	0.2047	0.7697	0.0000	1.0
1.0	0.0256	0.2047	0.3849	0.3848	0.5
2.0	0.0499	0.1996	0.0000	0.7505	0.0
2.0	0.0499	0.1996	0.3752	0.3753	0.5

Mixtures are prepared in stainless steel mixing tanks, 17 L and 15 L in size. The proportions of reactants in the mixture are determined by specifying the absolute mass of the fuel, the equivalence ratio, and the ratio of Ar : N<sub>2</sub> in the oxidizer. Mixtures are made by first vacuuming the mixing tanks to an ultimate pressure less than 5 Torr. Since MV is a liquid with a relatively small vapor pressure at room temperature and pressure, it is measured gravimetrically to within 0.01 g of the specified value. The fuel is injected into the mixing tank through a septum. Proportions of O<sub>2</sub>, Ar, and N<sub>2</sub> are added manometrically at room temperature and the total pressure is measured by an Omega Engineering MMA100V10T2D0T4A6 type static pressure transducer. The same transducer is used to measure the pressure of the reactant mixture prior to an experiment.

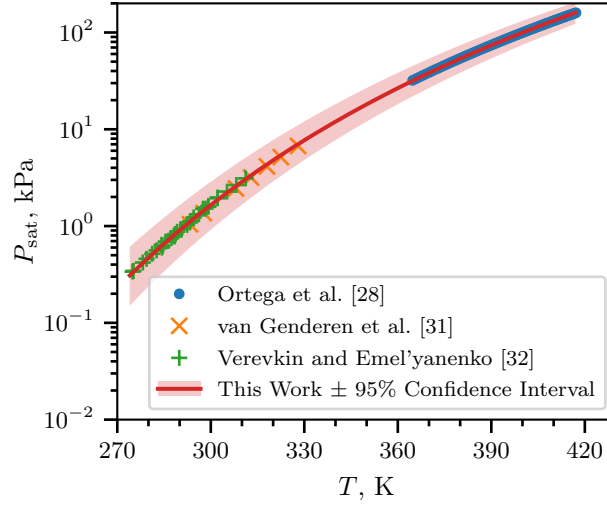
The RCM is equipped with heaters to control the initial temperature of the mixture. After filling in the components to the mixing tanks, the heaters are switched on and the system is allowed 1.5 h to come to steady state. The mixing tanks are also equipped with magnetic stir bars so the reactants are well mixed for the duration of the experiments. Previous work has shown this procedure to completely vaporize the fuel and prevent fuel cracking during the heating process [25–27].

The initial temperature is chosen such that the saturated vapor pressure ( $P_{\text{sat}}$ ) of the fuel at the initial temperature is at least twice the partial pressure of the fuel in the mixing tank. The Antoine equation

$$\log_{10} P_{\text{sat}} = A - \frac{B}{T - C} \quad (1)$$

is used to model the saturated vapor pressure of MV as a function of temperature ( $T$ ), where  $A$ ,  $B$ , and  $C$  are substance-specific coefficients, given in units of K and kPa. Coefficients for Eq. (1) are given in the literature by Ortega et al. [28], Camacho et al. [29], and Stephenson et al. [30]. Unfortunately, the values of the coefficients are different among all three references. Therefore, coefficients for use in Eq. (1) are determined in this work by least squares fitting of the data of Ortega et al. [28], van Genderen et al. [31], and Verevkin and Emel’yanenko [32] using the `curve_fit()` function of SciPy [22] version 0.19.0. Figure 2

119 shows that the coefficients fitted with this procedure give good agreement with  
 120 the experimental data; values for the coefficients computed in this work and  
 121 reported in the literature works are given in Table 2. The data and code used  
 122 to calculate the coefficients are provided in the Supplementary Material.



123

Figure 2: Saturated vapor pressure of MV as a function of temperature, plotted using the  
 124 Antoine equation, Eq. (1), with  $A = 6.4030$ ,  $B = 1528.69$ , and  $C = 52.881$ .

Table 2: Antoine Equation coefficients computed in this work and obtained from the literature,  
 in units of K and kPa. The  $2\sigma$  confidence interval is estimated by taking the square root of  
 125 the diagonals of the covariance matrix returned from `curve_fit()`

	$A$	$B$	$C$	$T_{\min}$ , K	$T_{\max}$ , K
This Work	6.4030	1528.69	52.881	274.9	417.18
$2\sigma$ Confidence Interval	0.0919	53.47	4.934	—	—
Ortega et al. [28]	6.23175	1429.00	62.30	364.75	417.18
Camacho et al. [29]	5.9644	1281.06	75.94	281	547
Stephenson et al. [30]	6.62646	1658.4	42.09	297	411

126

### 127 3. Computational Methods

#### 128 3.1. RCM Modeling

129 The Python 3.6 interface of Cantera [20] version 2.3.0 is used for all sim-  
130 ulations in this work. Detailed descriptions of the use of Cantera for these  
131 simulations can be found in the work of Weber and Sung [18] and Dames  
132 et al. [33]; a brief overview is given here. As mentioned in Section 2, non-  
133 reactive experiments are conducted to characterize the machine-specific effects  
134 on the experimental conditions in the RCM. This pressure trace is combined  
135 with the reactive pressure trace and used to compute a volume trace by as-  
136 suming that the reactants undergo a reversible, adiabatic, constant composition  
137 (i.e., isentropic) compression during the compression stroke and an isentropic  
138 expansion after the EOC. The volume trace is applied to a simulation con-  
139 ducted in an `IdealGasReactor` in Cantera [20] using the CVODES solver from  
140 the SUNDIALS suite [34]. The ignition delays from the simulations are de-  
141 fined in the same manner as in the experiments. The time derivative of the  
142 pressure in the simulation is computed by second order Lagrange polynomials,  
143 as discussed by Chapra and Canale [35]. The volume trace files, the corre-  
144 sponding pressure traces, and `volume-trace.yaml` files suitable for use with  
145 UConnRCMPy v3.0.5 [19] are available on the web at [https://combdialab.](https://combdialab.engr.uconn.edu/database/rcm-database)  
146 [engr.uconn.edu/database/rcm-database](https://combdialab.engr.uconn.edu/database/rcm-database) and on figshare at [https://doi.](https://doi.org/10.6084/m9.figshare.5213341)  
147 [org/10.6084/m9.figshare.5213341](https://doi.org/10.6084/m9.figshare.5213341). In addition, ChemKED-format [36] files  
148 are available in the main ChemKED database repository at [https://github.](https://github.com/pr-ometh-us/ChemKED-database)  
149 [com/pr-ometh-us/ChemKED-database](https://github.com/pr-ometh-us/ChemKED-database).

150 To the best of our knowledge, there are three mechanisms for MV combus-  
151 tion available in the literature. The first two, by Korobeinichev et al. [12] and  
152 Dmitriev et al. [13], were developed to simulate flames, and do not include the  
153 low-temperature chemistry necessary to simulate the conditions in the current  
154 RCM experiments. The third model was developed by Diévert et al. [15] and  
155 includes low-temperature chemistry of MV, although it was only validated by  
156 comparison with flame extinction limits. In converting this mechanism for use in



Cantera, we found that there were many species in the thermodynamic database with multiple data entries. For most of these species the thermodynamic data is identical. However, some species are not exact duplicates. For these species, it is not clear from the thermodynamic database file which data set should be preferred. Since Cantera (and CHEMKIN) choose the first instance of a duplicate species to be used, we retained the first entry for all duplicated species. The detailed model of Diévert et al. [15] includes 1105 species and 7141 reactions, and the Cantera formatted input file is available in the Supplementary Material.

### 3.2. Reaction Mechanism Generator

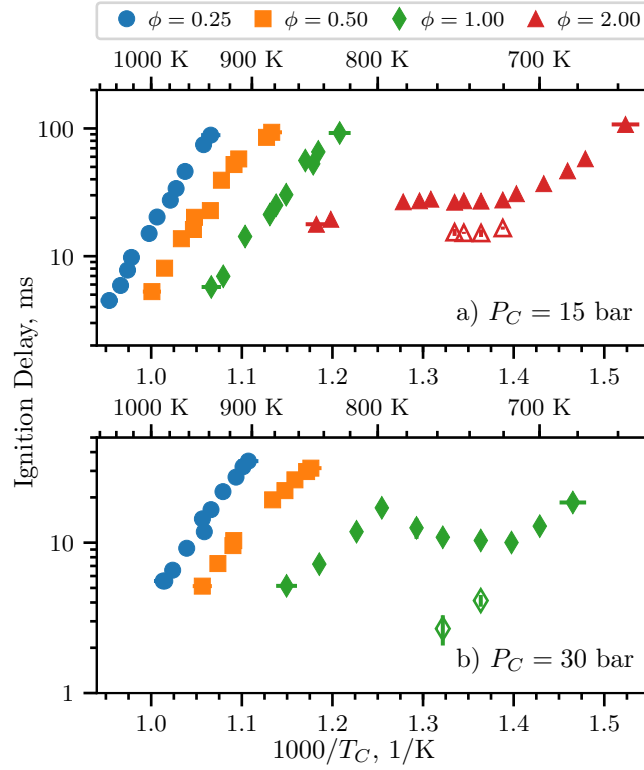
In addition to using a mechanism from the literature, we investigate the use of an automatic mechanism generator, the open-source Reaction Mechanism Generator (RMG) [37] version 2.1.0. The Python version of RMG is used, which requires Python 2.7, and version 2.1.0 of the RMG database is used. The final RMG model contains 427 species and 13640 reactions. Note that the number of species is much lower than the Diévert et al. [15] model because the RMG model focuses on only one fuel (MV), but the number of reactions is substantially higher. The input file used to generate the model is available in the Supplementary Material. In addition, the CHEMKIN and Cantera formatted input files for the RMG-generated model are available in the Supplementary Material.

## 4. Experimental Results

### 4.1. Ignition Delays

Figure 3 shows the ignition delay results measured in this study. Filled markers denote the overall ignition delay and hollow markers indicate the first-stage ignition delay. Vertical error bars are drawn on the symbols to represent the  $2\sigma$  uncertainty in the ignition delay; for many of the experiments, the uncertainty is approximately the same size as the data point, so the error bar is hidden. Horizontal error bars are shown on the first and last points of each equivalence

ratio indicating the estimated uncertainty in the EOC temperature of  $\pm 1\%$  [38].  
 Fig. 3a shows the results for a compressed pressure of 15 bar, while Fig. 3b shows  
 the results for a compressed pressure of 30 bar. Note that  $\phi = 2.0$  results were  
 not collected for 30 bar, so there are no red triangle data points in Fig. 3b. A  
 summary of the ignition delay data is available as a comma-separated value  
 file in the Supplementary Material, including the mixture conditions for each  
 experiment, the initial conditions, the compressed conditions, and the ignition  
 delays and their associated errors.



193

Figure 3: Ignition delays of MV as a function of inverse temperature for varying equivalence ratios. Filled points are the overall ignition delays and hollow points are the first stage ignition delays. a) 15 bar, b) 30 bar.

194

It can be seen from Fig. 3 that the ignition delays for the  $\phi = 0.25$  and 0.5 mixtures do not show an NTC region of the ignition delay for both of the pressures studied in this work. However, the  $\phi = 1.0$  mixture shows an NTC

197

198 region at  $P_C = 30$  bar between approximately 720 K and 800 K, with measured  
199 first-stage ignition delays at 733 K and 757 K. In addition, the  $\phi = 2.0$  mixture  
200 shows an NTC region of ignition delay at 15 bar from approximately 720 K to  
201 780 K, with measured first-stage ignition delays between 720 K and 750 K.

202 Hady-Ali et al. [9] also observed two-stage ignition of MV in stoichiometric  
203 mixtures, stating that “[m]ethyl pentanoate... was more reactive [than methyl  
204 butanoate] with a limit below which autoignition no longer occurs observed at  
205  $T_c = 670$  K and  $P_c = 11.4$  bar. At this temperature, the autoignition occurred  
206 in two stages with a clearly identified cool flame event.” However, we do not  
207 find two-stage ignition for the similar pressure of  $P_C = 15$  bar in this study.  
208 We note that the stated temperature of the experiment from the work of Hady-  
209 Ali et al. [9] (670 K) is much lower than the lowest temperature we considered  
210 in this work at 15 bar,  $\phi = 1.0$  (828 K). We did not conduct experiments at  
211 lower temperatures because the work of Mittal and Sung [17] showed that the  
212 temperature field in the RCM reaction chamber was uniform for approximately  
213 100 ms after the EOC, and our measured ignition delay at 15 bar,  $\phi = 1.0$ , and  
214 828 K is 92.14 ms.

215 However, we find NTC behavior of the overall ignition delay and two-stage  
216 ignition at the higher pressure of 30 bar, and at higher temperatures than those  
217 reported for two-stage ignition in the study of Hady-Ali et al. [9]. The trend  
218 of NTC behavior shifting to higher temperatures with increasing pressure can  
219 be seen in other classes of fuels. Kukkadapu et al. [39] found a similar trend  
220 in gasoline composed of iso-alkanes, n-alkanes, cyclo-alkanes, aromatics, and  
221 olefins. Kukkadapu et al. [39] attributed the shift of the NTC region to the  
222 reactions between the hydroperoxyalkyl radical (QOOH) and  $O_2$  becoming more  
223 dominant than the unimolecular decomposition of QOOH at higher pressures.  
224 Similar trends could occur for the hydroperoxyalkyl radicals of MV.

225 To further understand the effect of the methyl ester functional group on the  
226 NTC region of ignition delay, we compare with the alkane and alcohol with  
227 5-carbon alkyl chains, n-pentane and n-pentanol. n-Pentane and MV have the  
228 same fuel mole percentage for stoichiometric mixtures in air (2.56 %), while

229 n-pentanol has a fuel mole percentage of 2.72 % for stoichiometric conditions.  
 230 Ribaucour et al. [40] and Bugler et al. [41] found the NTC region for n-pentane  
 231 to be between 760 K and 910 K at pressures near 10 atm. As we will compare  
 232 with our MV data at 30 bar, we note that increasing the pressure tends to shift  
 233 the NTC to higher temperatures, as mentioned previously [39]. Heufer et al. [42]  
 234 found NTC behavior for n-pentanol in the range of 770 K to 900 K at 30 bar. In  
 235 this study, we find the NTC window for MV at 30 bar to be between 720 K and  
 236 800 K. Therefore, it appears that the methyl ester functional group causes the  
 237 NTC range to occur at lower temperature as compared to alkanes and alcohols  
 238 with similar alkyl chain lengths. This result was also noted by Hadj-Ali et al.  
 239 [9] for methyl hexanoate as the fuel.

#### 240 4.2. Pressure Traces

241 Figure 4a shows the pressure traces for selected experiments at  $\phi = 1.0$ ,  $P_C =$   
 242 30 bar. The three reactive pressure traces shown are at the low-temperature end  
 243 of the NTC (blue, 700 K), one case with two-stage ignition (orange, 733 K), and  
 244 one case near the high-temperature limit of the NTC region (green, 774 K). Also  
 245 shown is the non-reactive pressure trace for the 700 K case (red). By comparing  
 246 the 700 K pressure trace with the non-reactive pressure trace, it can be seen  
 247 that there is substantial heat release prior to main ignition as measured by the  
 248 deviation of the reactive pressure trace from the non-reactive trace. However,  
 249 there is only one peak in the time derivative of the pressure, so no first-stage  
 250 ignition delay is defined for this case. It can also be seen in Fig. 4a that the  
 251 774 K case shows some heat release prior to ignition, although again there is  
 252 only one peak in the time derivative of the pressure. Furthermore, the heat  
 253 release at 774 K appears to be more gradual than at 700 K.

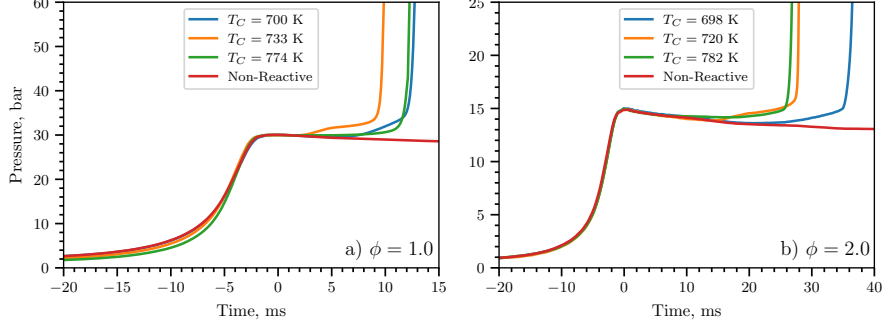


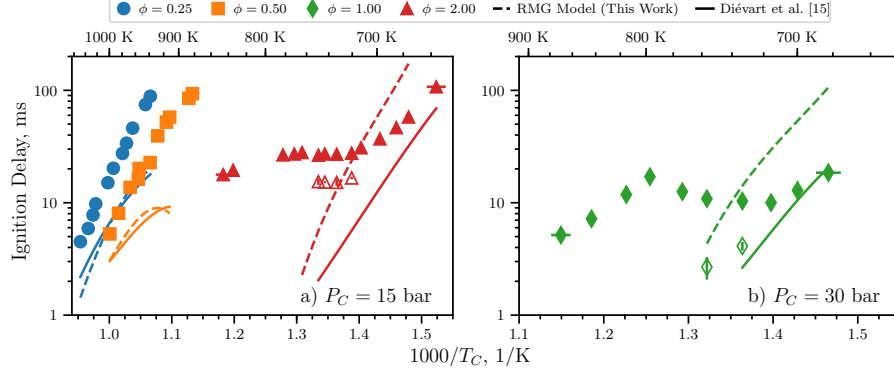
Figure 4: Selected pressure traces around the NTC region of ignition delay. a)  $\phi = 1.0$ ,  $P_C = 30$  bar, b)  $\phi = 2.0$ ,  $P_C = 15$  bar. The corresponding non-reactive pressure traces are also included for reference.

A similar trend can be observed in Fig. 4b for  $\phi = 2.0$  at  $P_C = 15$  bar, where pressure traces at several points around the NTC region are plotted. As in Fig. 4a, the three reactive pressure traces shown are at the low-temperature end of the NTC (blue, 698 K), one case with two-stage ignition (orange, 720 K), and one case near the high-temperature limit of the NTC region (green, 782 K). Also shown is the non-reactive pressure trace for the 698 K case (red). As for the  $\phi = 1.0$  case, the pressure traces show significant heat release prior to the overall ignition, as judged by deviation from the non-reactive case.

## 5. Computational Results

Figure 5 compares experimentally measured overall ignition delays with ignition delays computed with the detailed model of Diévar et al. [15] (solid lines). Figure 5a shows results at  $P_C = 15$  bar, while Fig. 5b shows results at  $P_C = 30$  bar. Only some equivalence ratios are shown for each pressure condition; data and simulated results are not shown for cases where the reactive simulated temperature at the EOC deviated substantially from the non-reactive temperature due to heat release during the compression stroke. Furthermore, it is important to note that the model of Diévar et al. [15] was not validated for MV ignition delays, only for extinction strain rates.

274



275

Figure 5: Comparison of experimental ( $\tau$  and  $\tau_1$ ) and simulated ( $\tau$ ) ignition delays computed using the procedure described in Section 3.1. a) 15 bar, b) 30 bar.

At 15 bar, the experimental overall ignition delays are under-predicted by the Diévert et al. [15] model for the three equivalence ratios shown. For the  $\phi = 0.25$  and 0.5 conditions, the model appears to be predicting an NTC region of the overall ignition delays as the temperature decreases, as judged by the increasing curvature of the simulations, although such a trend is not observed for the experimental data. However, at  $\phi = 2.0$ , the model does not predict the presence of an NTC region, although one is present in the experiments. Nonetheless, the agreement seems to be improving as the temperature is decreased. Comparing the Diévert et al. [15] model to the stoichiometric data at 30 bar, we find a similar trend as the  $\phi = 2.0$ ,  $P_C = 15$  bar data. The model does not predict the NTC region found experimentally for the  $\phi = 1.0$ ,  $P_C = 30$  bar experiments, but the agreement improves as the temperature decreases. Interestingly, two-stage ignition is predicted for all of the  $\phi = 1.0$  and  $\phi = 2.0$  data shown in Fig. 5. However, the first-stage ignition delays are 0.1 ms to 0.5 ms less than the overall ignition delays, and are not shown on Fig. 5 because they are nearly indistinguishable from the overall ignition delay.

To further understand the model of Diévert et al. [15], we have conducted adiabatic, constant volume simulations (called CONV simulations), as these simulations are not linked to a particular experiment by the volume trace and

can be conducted over a wide range of temperatures. In the CONV simulations, overall ignition delay is defined as an increase in the temperature of 400 K over the initial temperature. The diluent for all of the CONV simulations is pure argon, although the RCM simulations described previously consider the diluent mixture associated with each experiment (either pure argon or a 50:50 mixture of argon and nitrogen by mole, see Table 1 and the Supplementary Material).

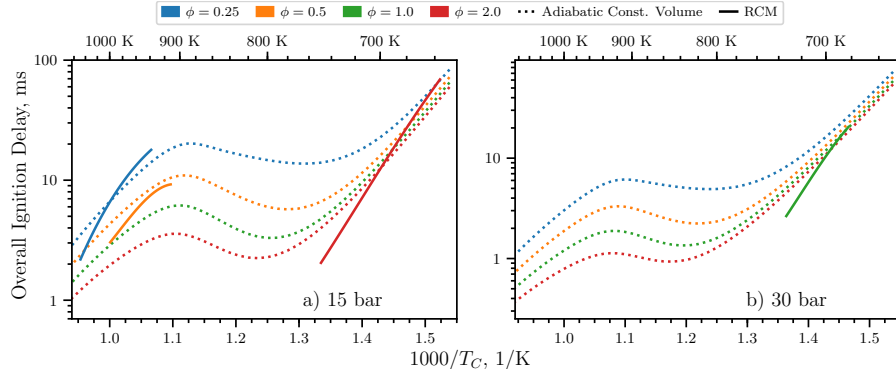


Figure 6: Comparison of simulated overall ignition delays computed in an adiabatic, constant volume system (dotted lines) and computed using the procedure described in Section 3.1 (solid lines). a) 15 bar, b) 30 bar.

Figure 6 compares the CONV simulations to the RCM simulations shown in Fig. 5. From Fig. 6, it can be seen that the curvature in the RCM simulations at  $P_C = 15$  bar,  $\phi = 0.25$  and  $0.5$  is related to the NTC region of the overall ignition delay, while the lack of curvature in the  $P_C = 15$  bar,  $\phi = 2.0$  and the  $P_C = 30$  bar,  $\phi = 1.0$  simulations is because those lie on the low-temperature side of the predicted NTC. It is clear from Fig. 6 that the model of Diévert et al. [15] predicts the NTC to occur at too high a temperature relative to the experiments.

To elucidate the underlying reasons for the disagreement between the Diévert et al. [15] model and the data, we conduct simulations with an additional model constructed using RMG (see Section 3.2). As can be seen in Fig. 5a, the agreement between the RMG model (dashed lines) and the experimental data is similar to the Diévert et al. [15] model for the  $P_C = 15$  bar,  $\phi = 0.25$  and  $0.5$

317 data. Moreover, the RMG model predicts a similar NTC region as temperature  
 318 is decreasing. For the  $P_C = 15$  bar,  $\phi = 2.0$  data, the RMG model tends to  
 319 over-predict the low-temperature overall ignition delays (i.e., those to the right  
 320 of the experimental NTC region on the Arrhenius plot), and does not predict the  
 321 NTC region found experimentally. As before, the trend at  $P_C = 30$  bar,  $\phi = 1.0$   
 322 is similar to the  $P_C = 15$  bar,  $\phi = 2.0$  data; the RMG model over-predicts the  
 323 low-temperature overall ignition delays and does not predict the experimental  
 324 NTC region. Finally, as in the Diévert et al. [15] model, two-stage ignition is  
 325 predicted for all of the  $\phi = 1.0$  and  $\phi = 2.0$  data shown in Fig. 5. However,  
 326 the first-stage ignition delays are 0.1 ms to 0.5 ms less than the overall ignition  
 327 delays, and are not shown on Fig. 5 because they are nearly indistinguishable  
 328 from the overall ignition delay.

329 It is clear that neither model is able to predict the ignition delays of MV  
 330 particularly well. In addition to the poor agreement shown in Fig. 5, the simu-  
 331 lations for  $P_C = 15$  bar,  $\phi = 1.0$  and  $P_C = 30$  bar,  $\phi = 0.25, 0.5$  and  $2.0$  showed  
 332 substantial heat release during the compression stroke (i.e., the simulations are  
 333 much too reactive), and so these conditions are not compared in Fig. 5. We note  
 334 again that the model by Diévert et al. [15] was validated for MV combustion  
 335 only by comparison to flame extinction limits, so the disagreement is not wholly  
 336 surprising.

337 In general, there could be three likely sources of error in the models: missing  
 338 reaction pathways, incorrect values of the reaction rates, and incorrect values  
 339 for thermodynamic properties of the species. We have noted in Section 3.2 that  
 340 the RMG model has many more reactions than the Diévert et al. [15] model  
 341 and the algorithm used in RMG considers a substantial number of the possible  
 342 pathways. This reduces the possibility of missing reaction pathways affecting  
 343 the model. Further detailed studies are required to ensure that the RMG model  
 344 includes all of the relevant reaction pathways, which are outside the scope of  
 345 this work.

346 The second source of error may be incorrect reaction rate parameters, either  
 347 because the rates are specified incorrectly in the model or because the rates are



not well estimated by the typical analogy based-rules. It should be noted that errors of this type may affect the model generated by RMG—if the rates are not estimated correctly, reactions that are important in reality may not be included in the model. Determining the accuracy of the reaction rates used in the RMG and Diévar et al. [15] models requires further detailed studies of the models, which are also outside the scope of this work. Another, related, source of error could be incorrect estimation of the pressure dependence of the reaction rates, which may be particularly important for the isomerization reactions prevalent in low-temperature chemistry.

The third source of error may lie in the estimation of the thermodynamic properties of the species, particularly the fuel radicals. In the work of Diévar et al. [15], the program THERM [43] was used to estimate thermodynamic values using the group additivity method. In the RMG model constructed in this work, RMG itself estimates the thermodynamic properties of the molecules also using the group additivity method. Nonetheless, the two models have differing predictions of the thermodynamic properties of the species in the model, particularly the fuel and its radicals. The values of the heats of formation of the fuel and its H-atom abstraction radicals are shown in Table 3; the radicals are labeled according to the convention shown in Fig. 7.

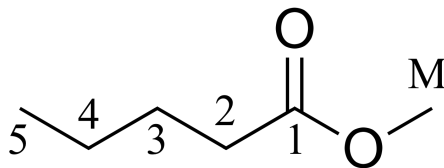


Figure 7: Structure of MV with carbon atoms labeled according to the convention used in Table 3 and Table 4

Table 3 shows that the heats of formation of the fuel and radicals 3, 4, 5, and M are quite similar between the two mechanisms. However, the heat of formation of the second radical, the one closest to the methyl ester group, has a significantly lower heat of formation in the model by Diévar et al. [15] than in the RMG model. Note that it is expected that the second radical will

374 be somewhat more stable than the other radicals, due to the influence of the  
 375 methyl ester group on the adjacent carbon atom.

Table 3: Heats of formation of MV and its radicals, labeled according to the convention used  
 376 in Fig. 7

Radical Site	Diévert et al. [15]		RMG Model (this work)	
	[kJ/mol]	[kcal/mol]	[kJ/mol]	[kcal/mol]
MV	-470.98	-112.57	-472.53	-112.94
2	-297.16	-71.02	-273.63	-65.40
3	-277.03	-66.21	-273.63	-65.40
4	-277.03	-66.21	-278.61	-66.59
5	-265.94	-63.56	-267.53	-63.94
M	-270.51	-64.65	-270.12	-64.56

378 This difference in heats of formation affects the pathways that consume the  
 379 fuel. By conducting a reaction pathway analysis to determine which radicals are  
 380 formed from the breakdown of the fuel, we can analyze the proportion of each  
 381 radical formed as the fuel breaks down during the autoignition process. The  
 382 following analysis is conducted for a constant volume, adiabatic simulation with  
 383 initial temperature and pressure of 700 K and 30 bar, respectively, and for the  
 384 stoichiometric equivalence ratio. The rates of production of the species have  
 385 been integrated until the time of 20 % fuel consumption. The results of this  
 386 analysis are shown in Table 4 for the two models. The percentages shown in  
 387 Table 4 are the percent of the fuel consumed to form a particular fuel radical  
 388 by all the reactions that can form that radical, and the radicals are labeled  
 389 according to the convention in Fig. 7.

390 At the relatively low temperature and high pressure condition of this analy-  
 391 sis, all of the fuel is consumed by H-atom abstractions to form the fuel radicals  
 392 shown. It can be seen that the two models have quite different distributions  
 393 of products from the first H-abstraction reactions. The model of Diévert et al.  
 394 [15] predicts that H-abstraction from the second carbon is the most prevalent,

while the RMG model predicts that the radical on the fourth carbon in the chain will be primarily formed. This is in line with the heats of formation in Table 3, where the most stable radical (i.e., the radical with the smallest heat of formation) is most likely to be formed in each model.

Table 4: Percent of MV consumed to form fuel radical species with a hydrogen atom missing at the location indicated in the first column and Fig. 7

Radical Site	Diévert et al. [15] [%]	RMG Model [%]	RMG switched [%]
2	29.2	12.5	11.0
3	17.5	12.2	11.1
4	17.5	50.6	56.6
5	9.5	3.9	4.3
M	26.3	20.8	16.9

To further compare the models with each other, the NASA polynomials representing the thermodynamic properties of MV and the 5 fuel radicals from the model of Diévert et al. [15] are used to replace the equivalent molecules in the RMG model. The results of a path analysis at the same condition as the other analysis is shown in Table 4 in the “RMG switched” column. The results of the analysis of the “RMG switched” model show that the radical on the fourth carbon is still the most prevalent, despite the heats of formation for the fuel radicals in the “RMG switched” model being identical to the Diévert et al. [15] model. This suggests that the reaction pathways have a substantial impact on the simulation, in addition to the influence of the thermochemistry, as discussed previously. Moreover, since the thermochemistry of the species in a reaction controls the reverse reaction rate of a reaction, the RMG algorithm may miss important pathways due to improperly estimated thermochemistry.

Taken together, these results show that the poor performance in a given model cannot be attributed to a single source. Separating the influence of thermochemistry and kinetics requires further detailed study of the methyl valerate system specifically, and methyl ester systems more generally. Although such

419 detailed work has begun, for example, with the work of Hayes and Burgess  
420 [14], further work is required to accurately predict the low temperature ignition  
421 delays of methyl valerate.

## 422 6. Conclusions

423 In this study, we have measured ignition delays for methyl valerate over a  
424 wide range of engine-relevant pressures, temperatures, and equivalence ratios.  
425 An NTC region of the overall ignition delay and two-stage ignition are recorded  
426 for pressures of 15 bar at  $\phi = 2.0$  and 30 bar at  $\phi = 1.0$ . A detailed chemical  
427 kinetic model available in the literature is unable to reproduce the experimental  
428 results, so a new model is constructed using the Reaction Mechanism Generator  
429 software. Although the new model contains many more reactions than the  
430 literature model, it is still unable to predict the experimental ignition delays  
431 satisfactorily. Both models predict an NTC region of the overall ignition delay  
432 under conditions where none is found in the experiments, and fail to predict  
433 the NTC region of overall ignition delay that is present in the experiments.  
434 Possible reasons for the discrepancy include missing reaction pathways, incorrect  
435 rate estimates, and incorrect thermodynamic property estimates. Comparative  
436 analysis of the two models failed to identify a single source of the error, and  
437 further detailed studies are required to improve predictions of the ignition delay  
438 at these engine-relevant conditions.

## 439 7. Acknowledgments

440 The authors acknowledge support from the Combustion Energy Frontier  
441 Research Center, an Energy Frontier Research Center funded by the U.S. De-  
442 partment of Energy, Office of Science, Office of Basic Energy Sciences, under  
443 award number DE-SC0001198.

## References

- [1] S. K. Hoekman, C. Robbins. Review of the effects of biodiesel on NO<sub>x</sub> emissions. *Fuel Processing Technology* 96 (2012) 237–249. doi:10.1016/j.fuproc.2011.12.036.
- [2] J. Y. Lai, K. C. Lin, A. Violi. Biodiesel combustion: Advances in chemical kinetic modeling. *Progress in Energy and Combustion Science* 37 (2011) 1–14. doi:10.1016/j.pecs.2010.03.001.
- [3] L. Coniglio, H. Bennadji, P. Glaude, O. Herbinet, F. Billaud. Combustion chemical kinetics of biodiesel and related compounds (methyl and ethyl esters): Experiments and modeling – Advances and future refinements. *Progress in Energy and Combustion Science* 39 (2013) 340–382. doi:10.1016/j.pecs.2013.03.002.
- [4] W. K. Metcalfe, S. Dooley, H. J. Curran, J. M. Simmie, A. M. El-Nahas, M. V. Navarro. Experimental and modeling study of C<sub>5</sub>H<sub>10</sub>O<sub>2</sub> ethyl and methyl esters. *The Journal of Physical Chemistry A* 111 (2007) 4001–4014. doi:10.1021/jp067582c.
- [5] S. M. Walton, M. S. Wooldridge, C. K. Westbrook. An experimental investigation of structural effects on the auto-ignition properties of two C<sub>5</sub> esters. *Proceedings of the Combustion Institute* 32 (2009) 255–262. doi:10.1016/j.proci.2008.06.208.
- [6] S. Dooley, H. J. Curran, J. M. Simmie. Autoignition measurements and a validated kinetic model for the biodiesel surrogate, methyl butanoate. *Combustion and Flame* 153 (2008) 2–32. doi:10.1016/j.combustflame.2008.01.005.
- [7] B. Akih-Kumgeh, J. M. Bergthorson. Comparative Study of Methyl Butanoate and n -Heptane High Temperature Autoignition. *Energy & Fuels* 24 (2010) 2439–2448. doi:10.1021/ef901489k.

- 471 [8] B. Akih-Kumgeh, J. M. Bergthorson. Structure-reactivity trends of C1–C4  
472 alkanoic acid methyl esters. *Combustion and Flame* 158 (2011) 1037–1048.  
473 doi:10.1016/j.combustflame.2010.10.021.
- 474 [9] K. Hadj-Ali, M. Crochet, G. Vanhove, M. Ribaucour, R. Minetti. A study  
475 of the low temperature autoignition of methyl esters. *Proceedings of the*  
476 *Combustion Institute* 32 (2009) 239–246. doi:10.1016/j.proci.2008.09.002.
- 477 [10] K. Kumar, C.-J. Sung. Autoignition of methyl butanoate under en-  
478 gine relevant conditions. *Combustion and Flame* 171 (2016) 1–14.  
479 doi:10.1016/j.combustflame.2016.04.011.
- 480 [11] E. Fisher, W. J. Pitz, H. J. Curran, C. K. Westbrook. Detailed chem-  
481 ical kinetic mechanisms for combustion of oxygenated fuels. *Proceed-*  
482 *ings of the Combustion Institute* 28 (2000) 1579–1586. doi:10.1016/S0082-  
483 0784(00)80555-X.
- 484 [12] O. Korobeinichev, I. Gerasimov, D. Knyazkov, A. Shmakov, T. Bolshova,  
485 N. Hansen, C. K. Westbrook, G. Dayma, B. Yang. An Experimental and  
486 Kinetic Modeling Study of Premixed Laminar Flames of Methyl Pentanoate  
487 and Methyl Hexanoate. *Zeitschrift für Physikalische Chemie* 229 (2015).  
488 doi:10.1515/zpch-2014-0596.
- 489 [13] A. M. Dmitriev, D. A. Knyazkov, T. A. Bolshova, A. G. Shmakov,  
490 O. P. Korobeinichev. The effect of methyl pentanoate addition on  
491 the structure of premixed fuel-rich n-heptane/toluene flame at at-  
492 mospheric pressure. *Combustion and Flame* 162 (2015) 1964–1975.  
493 doi:10.1016/j.combustflame.2014.12.015.
- 494 [14] C. Hayes, D. R. Burgess. Exploring the oxidative decompositions of methyl  
495 esters: Methyl butanoate and methyl pentanoate as model compounds for  
496 biodiesel. *Proceedings of the Combustion Institute* 32 (2009) 263–270.  
497 doi:10.1016/j.proci.2008.05.075.

- 498 [15] P. Diévar, S. H. Won, J. Gong, S. Dooley, Y. Ju. A comparative study  
499 of the chemical kinetic characteristics of small methyl esters in diffusion  
500 flame extinction. *Proceedings of the Combustion Institute* 34 (2013) 821–  
501 829. doi:10.1016/j.proci.2012.06.180.
- 502 [16] G. Mittal, C.-J. Sung. A Rapid Compression Machine for Chemical Kinetics  
503 Studies at Elevated Pressures and Temperatures. *Combustion Science and*  
504 *Technology* 179 (2007) 497–530. doi:10.1080/00102200600671898.
- 505 [17] G. Mittal, C.-J. Sung. Aerodynamics inside a rapid com-  
506 pression machine. *Combustion and Flame* 145 (2006) 160–180.  
507 doi:10.1016/j.combustflame.2005.10.019.
- 508 [18] B. W. Weber, C.-J. Sung. UConnRCMPy: Python-based Data Analy-  
509 sis for Rapid Compression Machines. in: S. Benthall, S. Rostrup (Eds.),  
510 *Proceedings of the 15th Python in Science Conference*, pp. 36–44. [http:](http://conference.scipy.org/proceedings/scipy2016/bryan_weber.html)  
511 [//conference.scipy.org/proceedings/scipy2016/bryan\\_weber.html](http://conference.scipy.org/proceedings/scipy2016/bryan_weber.html).
- 512 [19] B. W. Weber, R. Fang, C.-J. Sung. UConnRCMPy, 2017. v3.0.5.  
513 doi:10.5281/zenodo.815569.
- 514 [20] D. G. Goodwin, H. K. Moffat, R. L. Speth. Cantera: An Object-oriented  
515 Software Toolkit for Chemical Kinetics, Thermodynamics, and Transport  
516 Processes, 2017. v2.3.0. doi:10.5281/zenodo.170284.
- 517 [21] S. van der Walt, S. C. Colbert, G. Varoquaux. The NumPy Array: A  
518 Structure for Efficient Numerical Computation. *Computing in Science &*  
519 *Engineering* 13 (2011) 22–30. doi:10.1109/MCSE.2011.37.
- 520 [22] E. Jones, T. Oliphant, P. Peterson, et al. SciPy: Open source scientific  
521 tools for Python, 2001–. <https://scipy.org>.
- 522 [23] J. D. Hunter. Matplotlib: A 2D Graphics Environment. *Computing in*  
523 *Science & Engineering* 9 (2007) 90–95. doi:10.1109/MCSE.2007.55.

- [24] D. Lee, S. Hochgreb. Rapid Compression Machines: Heat Transfer and Suppression of Corner Vortex. *Combustion and Flame* 114 (1998) 531–545. doi:10.1016/S0010-2180(97)00327-1.
- [25] B. W. Weber, K. Kumar, Y. Zhang, C.-J. Sung. Autoignition of n-butanol at elevated pressure and low-to-intermediate temperature 158 (???) 809–819. doi:10.1016/j.combustflame.2011.02.005.
- [26] K. Kumar, G. Mittal, C.-J. Sung. Autoignition of n-decane under elevated pressure and low-to-intermediate temperature conditions 156 (???) 1278–1288. doi:10.1016/j.combustflame.2009.01.009.
- [27] A. K. Das, C.-J. Sung, Y. Zhang, G. Mittal. Ignition delay study of moist hydrogen/oxidizer mixtures using a rapid compression machine 37 (???) 6901–6911. doi:10.1016/j.ijhydene.2012.01.111.
- [28] J. Ortega, F. Espiau, J. Tojo, J. Canosa, A. Rodríguez. Isobaric Vapor-Liquid Equilibria and Excess Properties for the Binary Systems of Methyl Esters + Heptane. *Journal of Chemical & Engineering Data* 48 (2003) 1183–1190. doi:10.1021/jc030117d.
- [29] A. G. Camacho, J. M. Moll, S. Canzonieri, M. A. Postigo. Vapor-Liquid Equilibrium Data for the Binary Methyl Esters (Butyrate, Pentanoate, and Hexanoate) (1) + Propanenitrile (2) Systems at 93.32 kPa. *Journal of Chemical & Engineering Data* 52 (2007) 871–875. doi:10.1021/jc060469v.
- [30] R. M. Stephenson, S. Malanowski, D. Ambrose, Handbook of the Thermodynamics of Organic Compounds, Elsevier, New York, 1987.
- [31] A. C. van Genderen, J. van Miltenburg, J. G. Blok, M. J. van Bommel, P. J. van Ekeren, G. J. van den Berg, H. A. Oonk. Liquid–vapour equilibria of the methyl esters of alkanolic acids: Vapour pressures as a function of temperature and standard thermodynamic function changes. *Fluid Phase Equilibria* 202 (2002) 109–120. doi:10.1016/S0378-3812(02)00097-3.



- 551 [32] S. P. Verevkin, V. N. Emel'yanenko. Transpiration method: Vapor pres-  
552 sures and enthalpies of vaporization of some low-boiling esters. *Fluid Phase*  
553 *Equilibria* 266 (2008) 64–75. doi:10.1016/j.fluid.2008.02.001.
- 554 [33] E. E. Dames, A. S. Rosen, B. W. Weber, C. W. Gao, C.-J. Sung,  
555 W. H. Green. A detailed combined experimental and theoretical study  
556 on dimethyl ether/propane blended oxidation. *Combustion and Flame* 168  
557 (2016) 310–330. doi:10.1016/j.combustflame.2016.02.021.
- 558 [34] A. C. Hindmarsh, P. N. Brown, K. E. Grant, S. L. Lee, R. Serban, D. E.  
559 Shumaker, C. S. Woodward. SUNDIALS: Suite of nonlinear and differen-  
560 tial/algebraic equation solvers. *ACM Transactions on Mathematical Soft-*  
561 *ware* 31 (2005) 363–396. doi:10.1145/1089014.1089020.
- 562 [35] S. C. Chapra, R. P. Canale, *Numerical Methods for Engineers*, McGraw-  
563 Hill Higher Education, Boston, 6th ed edition, 2010.
- 564 [36] B. W. Weber, K. E. Niemeyer. ChemKED: A human- and machine-readable  
565 data standard for chemical kinetics experiments. Submitted to: *Interna-*  
566 *tional Journal of Chemical Kinetics* (2017). [arXiv:1706.01987](https://arxiv.org/abs/1706.01987).
- 567 [37] J. W. Allen, C. F. Goldsmith, W. H. Green. Automatic estimation of  
568 pressure-dependent rate coefficients. *Physical Chemistry Chemical Physics*  
569 14 (2012) 1131–1155. doi:10.1039/c1cp22765c.
- 570 [38] B. W. Weber, C.-J. Sung, M. W. Renfro. On the uncertainty of temperature  
571 estimation in a rapid compression machine. *Combustion and Flame* 162  
572 (2015) 2518–2528. doi:10.1016/j.combustflame.2015.03.001.
- 573 [39] G. Kukkadapu, K. Kumar, C.-J. Sung, M. Mehl, W. J. Pitz. Exper-  
574 imental and surrogate modeling study of gasoline ignition in a rapid  
575 compression machine. *Combustion and Flame* 159 (2012) 3066–3078.  
576 doi:10.1016/j.combustflame.2012.05.008.
- 577 [40] M. Ribaucour, R. Minetti, L. R. Sochet. Autoignition of n-pentane  
578 and 1-pentene: Experimental data and kinetic modeling. *Symposium*

- 579 (International) on Combustion 27 (1998) 345–351. doi:10.1016/S0082-  
580 0784(98)80422-0.
- 581 [41] J. Bugler, K. P. Somers, E. J. Silke, H. J. Curran. Revisiting the Ki-  
582 netics and Thermodynamics of the Low-Temperature Oxidation Pathways  
583 of Alkanes: A Case Study of the Three Pentane Isomers. The Journal of  
584 Physical Chemistry A 119 (2015) 7510–7527. doi:10.1021/acs.jpca.5b00837.
- 585 [42] K. A. Heufer, J. Bugler, H. J. Curran. A comparison of longer alkane  
586 and alcohol ignition including new experimental results for n-pentanol and  
587 n-hexanol. Proceedings of the Combustion Institute 34 (2013) 511–518.  
588 doi:10.1016/j.proci.2012.05.103.
- 589 [43] E. R. Ritter, J. W. Bozzelli. THERM: Thermodynamic property estimation  
590 for gas phase radicals and molecules. International Journal of Chemical  
591 Kinetics 23 (1991) 767–778. doi:10.1002/kin.550230903.